Nature Environment and Pollution Technology
An International Quarterly Scientific Journal

p-ISSN: 0972-6268
(Print copies up to 2016)
e-ISSN: 2395-3454

Vol. 21 | No. 2 | pp. 867-881 | 2022

Original Research Paper

https://doi.org/10.46488/NEPT.2022.v21i02.050

Open Access Journal

Adopting Gram-Schmidt and Brovey Methods for Estimating Land Use and Land Cover Using Remote Sensing and Satellite Images

Fatima Hashim*, Hayder Dibs† and Hussein Sabah Jaber***
*Surveying Engineering Department, College of Engineering, University of Baghdad, Baghdad, Iraq
**Al-Qasim Green University, Water Resources Engineering Faculty, Water Resources Management Engineering Department, Babylon, Iraq
†Corresponding author: Hayder Dibs; dr.hayderdibs@wrec.uoqasim.edu.iq

Nat. Env. & Poll. Tech.
Website: www.neptjournal.com

Received: 13-07-2021
Revised: 26-08-2021
Accepted: 01-10-2021

Key Words:
Image fusion
Support vector machine
Brovey method
Gram-Schmidt method

ABSTRACT

The production of Land Use and Land Cover thematic maps using remote sensing data is one of the things that must be dealt with carefully to obtain accurate results, data is obtained from sensors of different characteristics. It is not possible to obtain high spatial and spectral accuracy in one image, so we used a fusion image (multispectral image with a low spatial resolution with a panchromatic image with high spatial resolution), which achieved high efficiency in improving the methods of producing Land Use and Land Cover maps. In this study, we used Landsat-8 multispectral and panchromatic images. The study aims to investigate the effectiveness of panchromatic images in improving the methods of producing Land Use and Land Cover maps for the city of Karbala, Iraq. The Support Vector Machine was used to classify the fusion images using the Brovey method and Gram-Schmidt sharpening algorithms. The appropriate methodology for producing Land Use and Land Cover maps was suggested by comparing classifying results and the classification accuracy was evaluated through the confusion matrix. Where the results showed that the method of classifying the fused image by Gram-Schmidt and classified by Support Vector Machine is the best way to produce Land use and Land cover maps for the study area and achieved the highest results for overall accuracy and kappa coefficient of 97.81% and 0.95, respectively.

INTRODUCTION

One of the most important applications of remote sensing is the classification of satellite images, which have formed a wide range, especially in the production of Land Use/Land Cover (LU/LC) maps (Dibs 2013, Bouaziz et al. 2017, Dibs 2018) and in many applications such as land use discovery, natural hazard modeling, and urban expansion studies as well as for continuous updating of geospatial data (Sang et al. 2014, Otukei et al. 2015, Dibs et al. 2018) and monitoring of wetland degradation studies (Ali & Jaber 2020, Hasan et al. 2020a). For mapping LU/LC, it was found that the best method is to classify images and it is a complex process that depends on many concepts, including determining the appropriate classification method (Chasmer et al. 2014), training site, image processing, feature identification, post-classification processing and accuracy evaluation (Sang et al. 2014). Choosing the appropriate classifier is very important to achieve a satisfactory result in classifying the study area, many algorithms and techniques have been adopted to estimate classification, such as Support Vector Machine (SVM) (Iounousse et al. 2015) and other algorithms Artificial Neural Networks (DNN) (Cavur et al. 2015), Decision trees (DT) (Chasmer et al. 2014), and Maximum Likelihood (ML) (Gevana et al. 2015). Remote sensing data integration technologies (Gevana et al. 2015, Abbas & Jabber 2020, Hasab et al. 2020b) and Methods for fusion images from a set of multiple and different remote sensing data are one way to improve the accuracy of the data used to produce LU/LC maps, where many researchers dealt with methods and techniques for fusion multispectral (MS) image with a low spatial resolution with high spatial resolution panchromatic (Pan) image to obtain images with high spatial and spectral resolution (Dibs et al. 2020, Dibs et al. 2021). It used many sharpening algorithms such as the Brovey method, Gram-Schmidt (GS), Intensity-Hue-saturation (IHS), and Principle Component Analysis (PCA). (Tabib Mahmoudi & Karami 2020). Fusion methods and techniques have had a wide resonance in many applications that used multiple data and from different sources (Jawak & Luis 2013, Sameen et al. 2016, Dibs & Al-Hedny 2019, Dibs et al. 2020). Since the methods and algorithms of sharpening to combine images with rapid development in some applications such as classification of images, studying changes, and identifying features, the efficiency of sharpening algorithms were considered one of the

necessary things, which is to preserve the characteristics of the entered information (Tabib Mahmoudi & Karami 2020). Mandhare et al. (2013) used several sharpening algorithms such as IHS, Brovey, averaging method, and multiplier method to improve the spatial and spectral resolution of the merged images. Sarp (2014), also discussed the performance of four sharpening algorithms (GS, IHS, PCA, Brovey) for fusion MS and Pan images and found that PCA and GS work well in all technologies. Another scientist (Zhang et al. 2016), conducted a study to obtain images with high spatial resolution while maintaining the spectral distortion as less as possible using sharpening algorithms (Brovey, GS, PCA, and IHS) and by comparing the results, it was found that Brovey is the best. the objective of this research is to obtain an improved methodology for producing LU/LC maps within the study area.

MATERIALS AND METHODS

To produce and detect LU/LC maps, methods were selected and examined through previous works to ensure their effectiveness and accuracy in this field because the selected algorithms must be effective and achieve good results within the study area (Jia et al. 2014). In this study, Landsat-8 OLI (multispectral images with a spatial resolution of (30 m) and a panchromatic image with a spatial resolution of (15 m), which were obtained on July 13, 2020, were selected for the processing steps as in the pre-processing, layer stacking of images was performed using bands (1, 2 & 3), and sub-setting was done to define the study area to reduce storage size and to facilitate the recall of files. Processing stage the images were corrected from geometric and radiometric errors to prepare the images for further processing. Later, the process of fusion image was conducted using the multispectral image with the panchromatic image with the use of two fusion approaches, the Brovey method sharpening algorithm and the other once the Gram-Schmidt (GS) sharpening algorithm and two fused images were obtained. To complete the processing and analysis operations to produce LU/LC maps, the classification of the two fused images was carried out using the SVM algorithm. The accuracy was evaluated based on the confusion matrix, and to determine the best methodology to improve the production of LU/LC maps for the study area, a comparison was made between the classification results. Fig. 1 shows a diagram of the methodology used for this study.

Study Area

The study area is the city of Karbala, Iraq, and it is one of the important Iraqi governorates because of its economic and tourism importance. Its location is between longitude 44°02′- 44°40′ E and latitude of 32°37′- 33° 31′ N. It has an area of 5,034 km^2 and a population of about 1.219 million in 2018. Karbala's climate is predominantly desert, with temperatures in summer reaching 45° and dropping to zero degrees in winter. It is one of the Iraqi cities with good economic returns due to its orchards of various types of crops such as dates, fruits, vegetables, and wheat. It is also famous for its handicrafts such as ceramics, as well as the manufacture of bricks and tiles. Karbala is a tourist city with a good financial return, which is frequented by tourists from all over the world to visit the holy sites (Jasem & AL-Mayali 2020). Fig. 2 shows the study area map.

The Dataset

The data that was used in this study includes the data set of the Landsat- 8 OLI satellite, recorded on July 13, 2020. The Landsat satellite includes two sensors, one of which is an operational land imaging device (OLI), whose data was used, and the other is a thermal infrared sensor (TIRS). The Landsat satellite data consists of 11 bands, where bands (1-7, 9) have a spatial resolution of (30) meters, and band (8) represents Pan and its spatial accuracy (15) meters, while bands 11 and 10 have infrared thermal radiation and have a spatial accuracy of (100) meters. Tables 1 &2 show the characteristics of OLI and TIRS (https://www.usgs.gov/

Table 1: Technical characteristics of OLI of Landsat-8.

Bands	Wavelength [mm]	Resolution [m]
Band 1- visible	0.43 - 0.45	30
Band 2- visible	0.45 - 0.51	30
Band 3 -visible	0.53 - 0.59	30
Band 4- near infrared	0.64 - 0.67	30
Band 5- near infrared	0.85 - 0.88	30
Band 6- SWIR	1.57 - 1.65	30
Band 7 -SWIR	2.11 - 2.29	30
Band 8 panchromatic	0.50 - 0.68	15
Band 9 cirrus	1.36 - 1.38	30

(source: https://www.usgs.gov/media/images/landsat-8-band-designations)

Table 2: Technical specification of TIRS of Landsat-8.

Band name	Central wavelength [μm]	Spectral range [μm]	Spatial resolution [m]
Band 10 / TIRS-1	10.9	10.6–11.19	100
Band 11 / TIRS-2	12.0	11.5–12.5	100

(source: https://www.usgs.gov/media/images/landsat-8-band-designations)

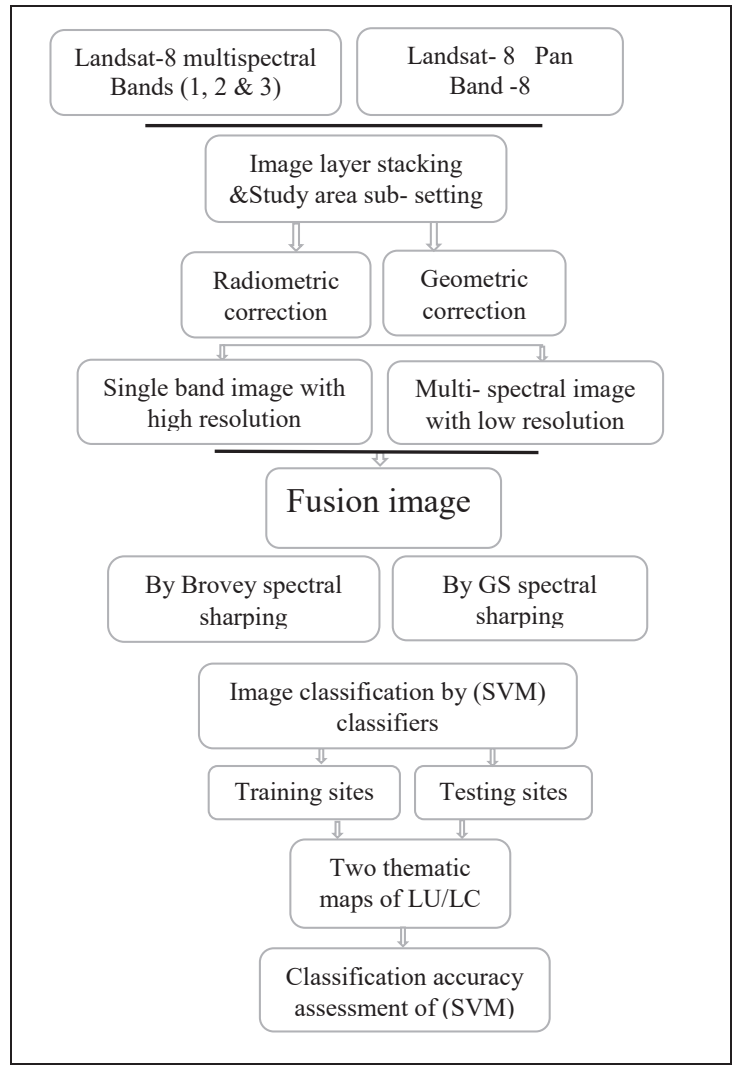

Fig. 1: Flowchart of methodology.

media/images/landsat-8-band-designations). The data was obtained free of charge from the US Geological Survey USGS website as a reference from (http://earthexplorer.usgs.gov) where we used Landsat -8 OLI (MS and Pan) satellite images, as shown in Fig. 3 & 4 showing the images used. We relied on google maps to match the data and choose training sites because they have high spatial accuracy.

Analysis and Processing

In this paper, we started by performing the processing steps, which include (1) pre-processing, which is layer stacking, and image sub-setting. (2) In the Processing steps, geometric and radiometric correction is applied to prepare the image for further processing and analysis, the geometric correction was carried out to reduce the geometric errors that cause different locations and the geometric correction was done using the image-to-image method depending on the ground control points (GCPs) from Fieldwork. The Landsat-8 (Pan) image with a spatial resolution of (15 m) and projected on the projection UTM, 38N, and WGS 84 Datum was considered error-free, and the geometric corrected based on ten ground control points. Table 3 shows the ground control points used and Fig. 5 shows the distribution of points in the study area. Root Mean Square Error (RMSE) was used as a measure of the variance between the measured and the predicted values, where the value of the RMSE was equal to 0.344, Table 4 shows the processing geometric for the Landsat-8 satellite image, and the geometric correction was made using the ENVI v5.3 program. A radiometric correction was carried out to remove the effects of sunlight, as several studies

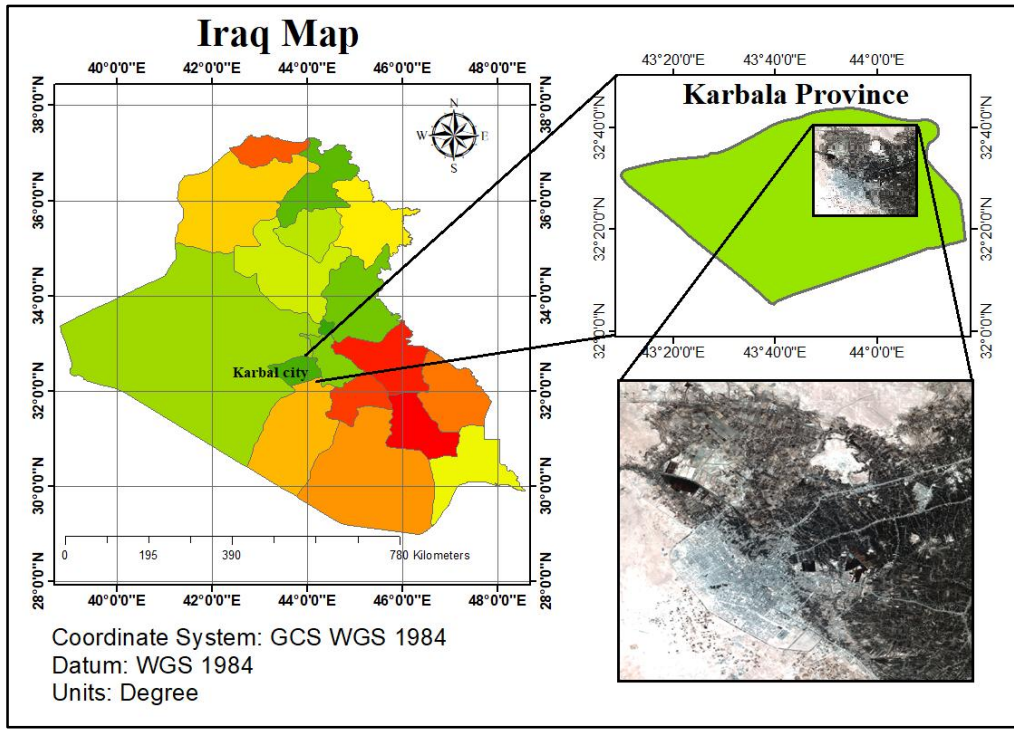

Fig. 2: The study area map.

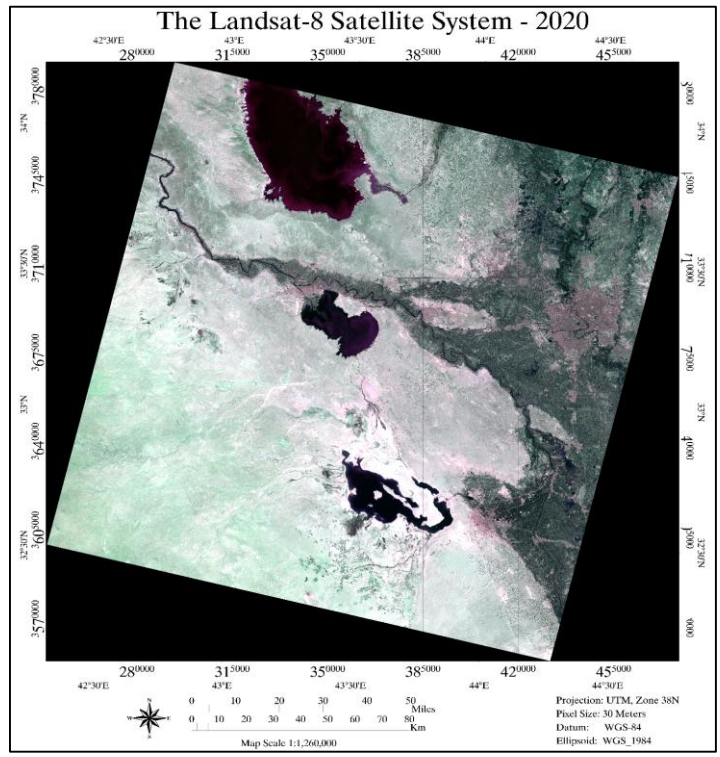

Fig. 3: Landsat-8 satellite (MS) image.

Table 3: Ground control points in the study area.

No.	Latitude	Longitude
1	32° 46′ 59.42"N	43° 55′ 43.42" E
2	32° 42′ 21.88" N	43° 54′ 27.08"E
3	32° 34′ 48.29" N	43° 58′ 38.72"E
4	32° 45′ 36.53" N	44° 06′ 22.25"E
5	32° 41′ 41.34" N	44° 11′ 48.61"E
6	32° 34′ 47.79" N	44° 11′ 42.31" E
7	32° 32′ 41.11" N	44° 03′ 50.24" E
8	32° 36′ 42.22" N	44° 03′ 37.64"E
9	32° 36′ 58.40" N	44° 04′ 11.52"E
10	32° 42′ 30.72" N	43°59′ 55.74"E

confirmed that it is one of the main methods of processing (Idi & Nejad 2013). The radiometric correction was done using the Quick Atmospheric Correction (QUAC) method. This method works to return the optical depth based on the spectra of the observed pixels available in the scene (Bernstein et al. 2012). Fig. 6 shows the corrected Pan image, and Fig. 7 shows the corrected MS image from (geometric and radiometric) errors.

Fusion Image

The fusion process of (MS and Pan) images was performed after pre-processing (layer stacking and image sub-setting) and processing (geometric and radiometric correction), two approaches were applied by performing image fusion between the (MS & Pan) dataset (Li et al. 2012, Idi & Nejad 2013, Löw et al. 2015). The first level of fusion between (MS& Pan) images was applied using the sharpening method (BT). which is a chromatic conversion method using three spectral bands, was applied to the fusion process, the aim of which is to print the three multispectral bands used to display RGB (Mandhare et al. 2013). The second approach used for data fusion is the GS method to improve spatial resolution (Kumar et al. 2014). The GS method calculates the average of the multispectral image bands and selects a range from the Pan image similar to the multispectral image bands. The mid-ranges of the multispectral image are replaced by the corresponding range of the Pan, and finally, the process is repeated in the opposite direction to obtain a high spatial resolution (Jawak & Luis 2013), The Fig. 8 shows the fusion of (MS & Pan) images using the BT sharpening algorithm, and Fig. 9 shows the fusion (MS & Pan) images using the GS sharpening algorithm.

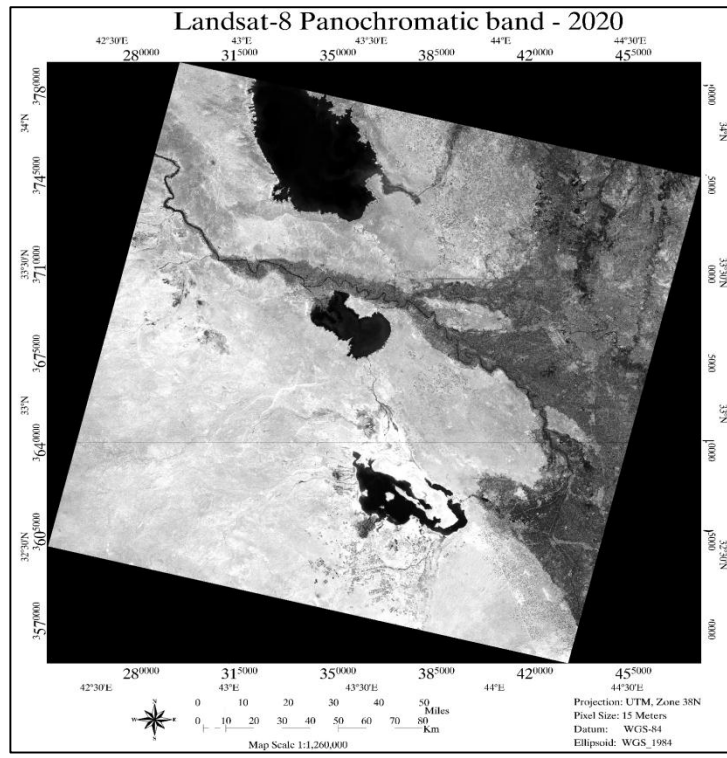

Fig. 4: Landsat-8 satellite (Pan) image.

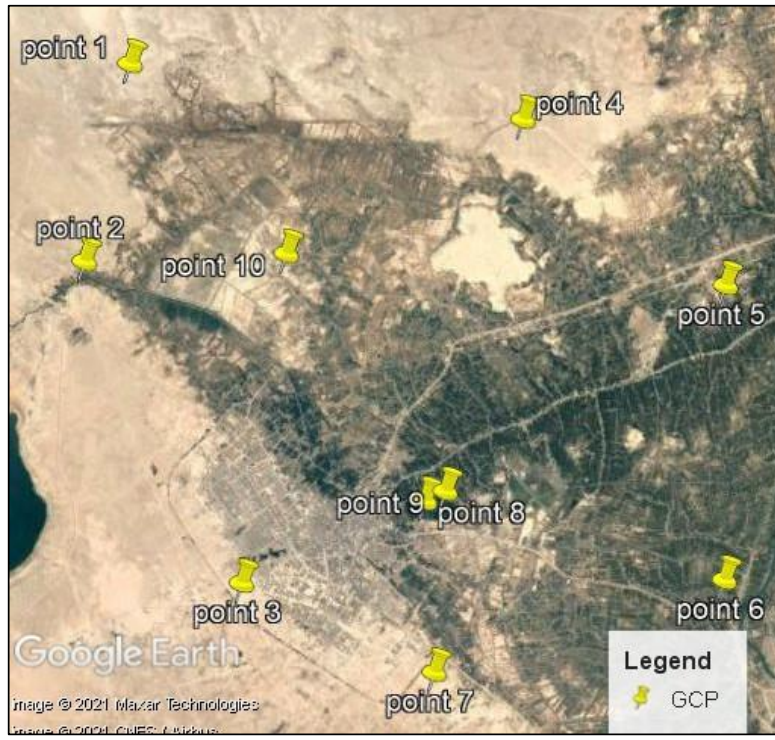

Fig. 5: The location of GCPs by Google earth.

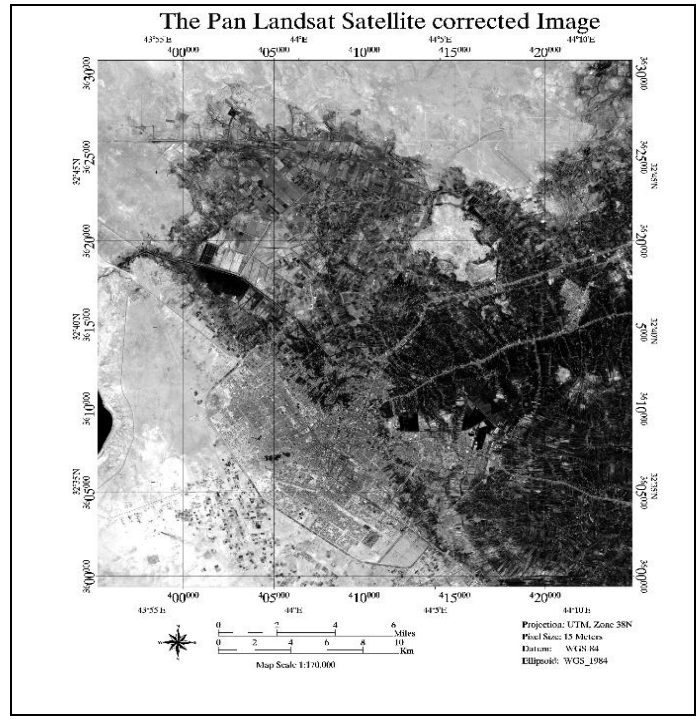

Fig. 6: Corrected Pan image.

Image Classification

After completing the processing operations and fusion of the (MS & Pan) images, the processing must be completed to produce LU/LC maps. The classification was applied to the fused images using supervised classification and by applying the SVM algorithm. The classification was performed according to the following steps:

Selecting Training and Testing Sites

Before starting the classification process, the study area was divided into six categories: urban area, vegetation, water bodies, soil-1, soil-2, and roads. Training samples were taken from the categories of the study area by selecting the polygons of the area of interest using ENVI v5.3. Fig. 10 shows the training sites for each category of the study area, and Table 5 gives the pixels that were chosen as training sites. Then the classification was applied using SVM and then the test samples were taken to verify the quality of the classification and its conformity with the study area.

Support Vector Machine

The SVM classification algorithm was applied in this study. SVM works to find the optimal separator to achieve the ideal classification by creating more than one separator and defining the super separator and depending on the experience of the analyzer as well as the pixels that were previously identified from the study area classes (Erener 2013). The classification was applied using SVM on the fused images by BT and GS sharpening algorithms after the study area was divided into six categories and training sites were selected and the kernel used for SVM was radial, Figs. 11 & 12 show the SVM parameters used to classify fused images using the (BT & GS) sharpening algorithms. Figs. 13 & 14 show LU/LC map classified using SVM classified on fused data by (BT & GS) methods

Accuracy Assessment

To assess the accuracy of the classification results we use the confusion matrix approach which is the most widely used method for assessing the accuracy of the classified data (Li et al. 2012). The accuracy of the SVM classifier used in this study was evaluated, and the kappa coefficient and overall accuracy were also used as an indicator to assess the accuracy, the Overall Accuracy (OA) and the Kappa coefficient can be calculated using equations 1 & 2 below (Dibs et al. 2021 and 2022).

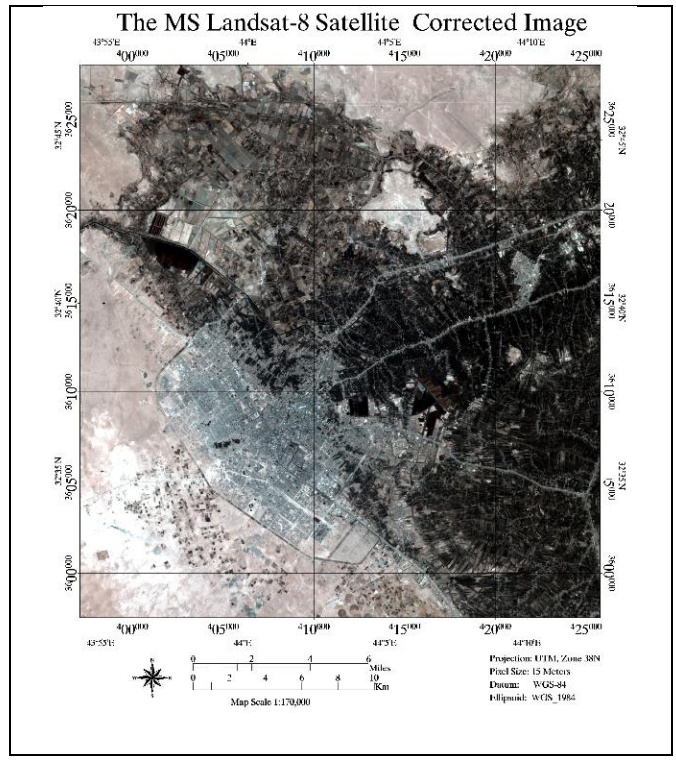

Fig. 7: Corrected MS image from (geometric and radiometric) errors.

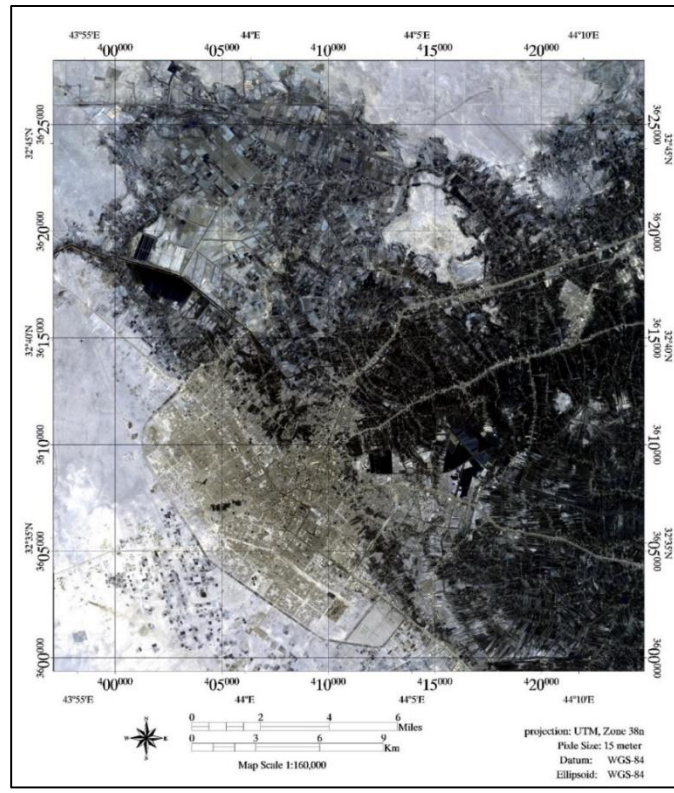

Fig. 8: Fusion image by Brovey method sharpening algorithm.

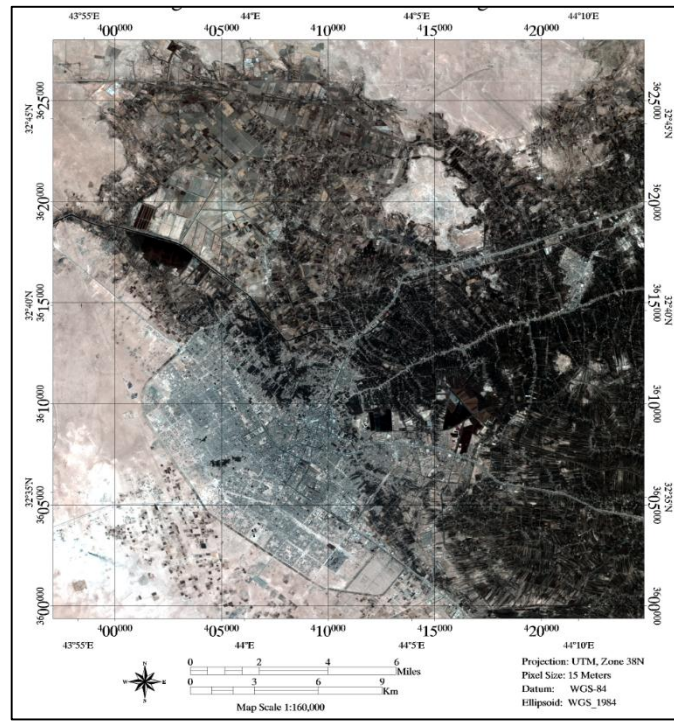

Fig. 9: Fusion image by Gram-Schmidt sharpening algorithm.

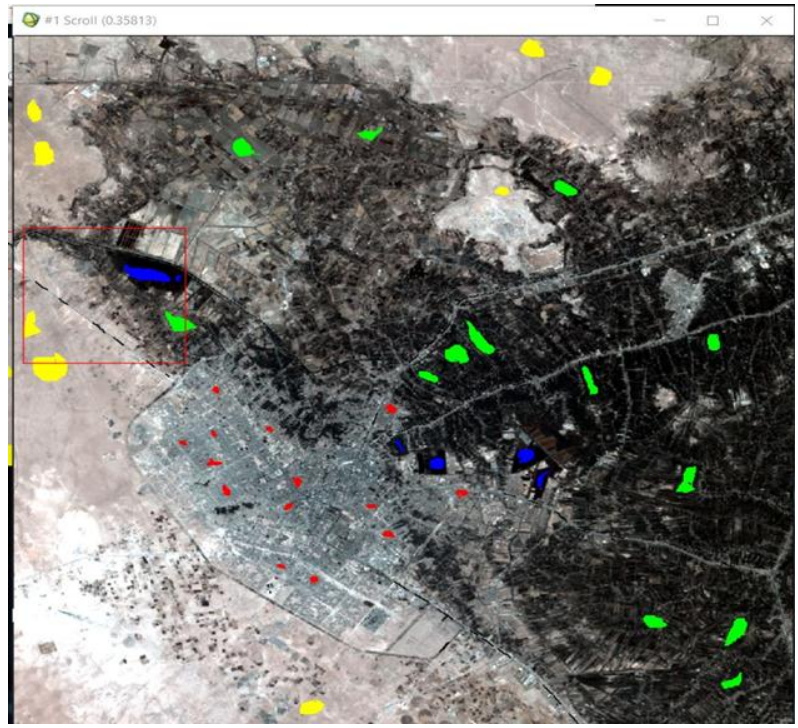

Fig. 10: location of training sites for the study area.

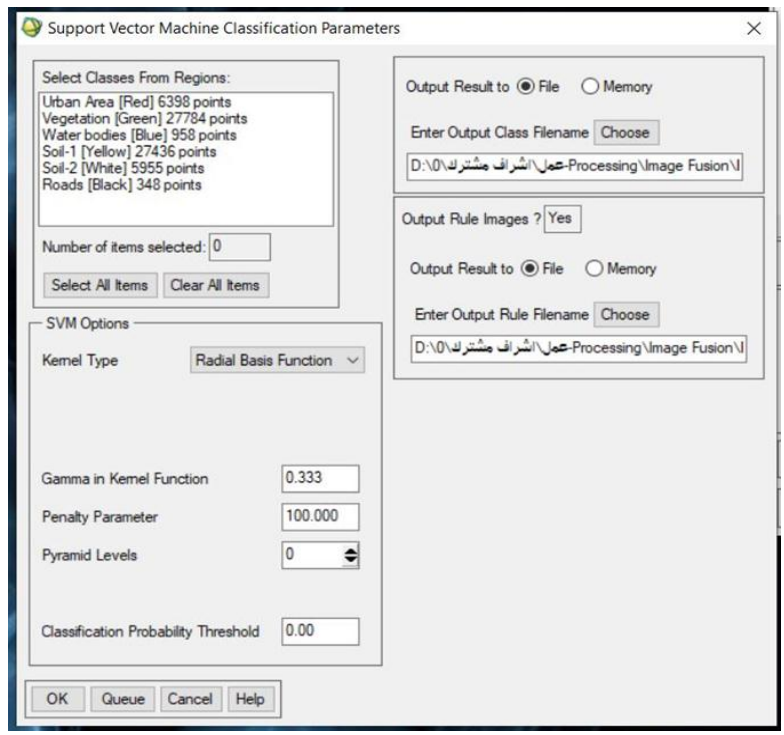

Fig. 11: SVM parameter for image fusion by (BT).

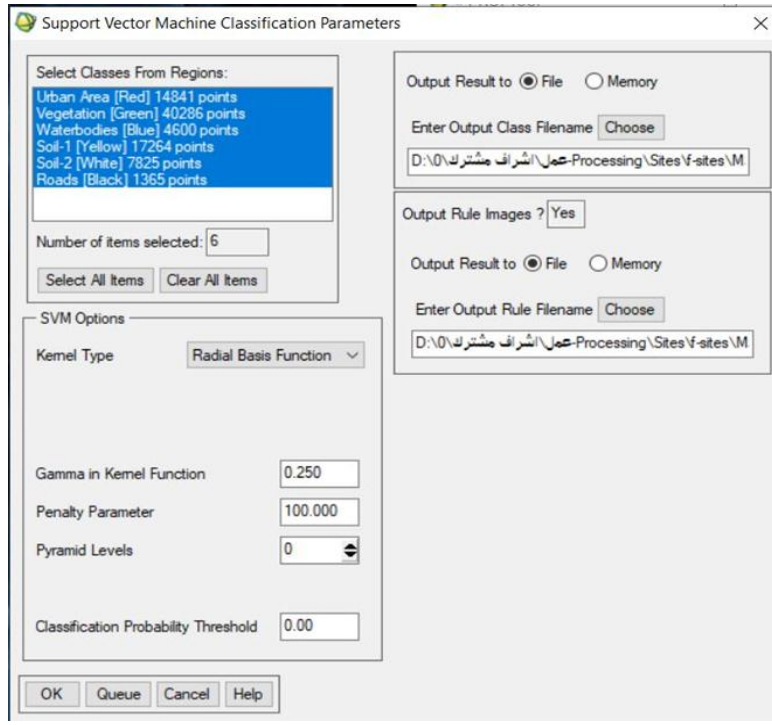

Fig. 12: SVM Parameter for image fusion by (GS).

$$\text{Kappa} = \frac{\sum_{i=1}^{c} n_{ij} - \sum_{i=1}^{c} n_i + n + i}{n^2 - \sum_{i=1}^{c} n_j + n + i} \quad \ldots(1)$$

$$\text{OA} = \frac{\sum_{i=1}^{c} n_{ij}}{n} \quad \ldots(2)$$

Table 4: Processing geometric correction for Landsat-8 image.

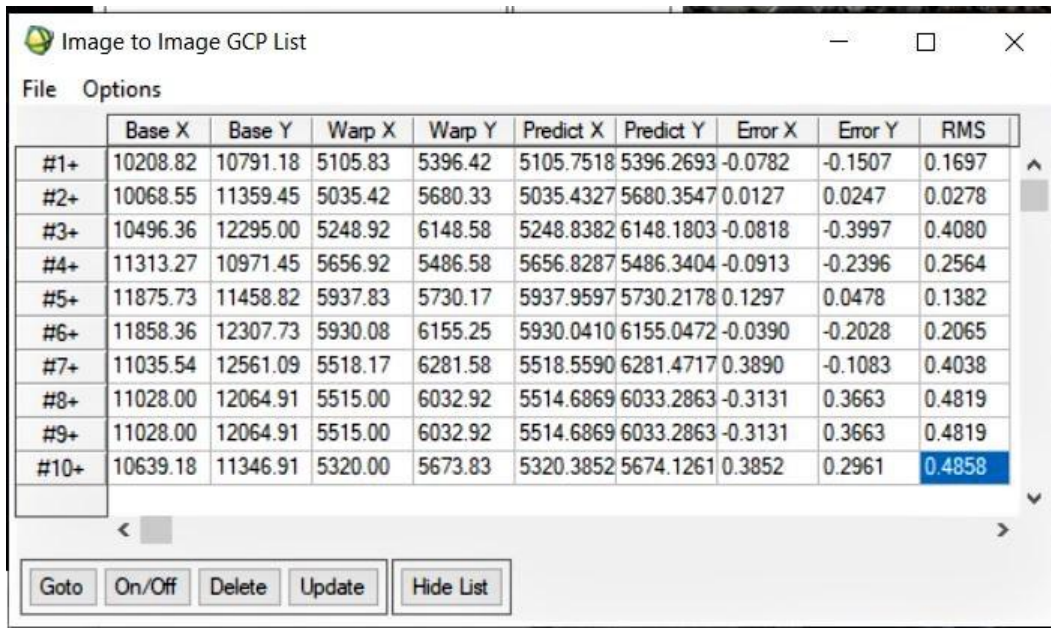

	Base X	Base Y	Warp X	Warp Y	Predict X	Predict Y	Error X	Error Y	RMS
#1+	10208.82	10791.18	5105.83	5396.42	5105.7518	5396.2693	-0.0782	-0.1507	0.1697
#2+	10068.55	11359.45	5035.42	5680.33	5035.4327	5680.3547	0.0127	0.0247	0.0278
#3+	10496.36	12295.00	5248.92	6148.58	5248.8382	6148.1803	-0.0818	-0.3997	0.4080
#4+	11313.27	10971.45	5656.92	5486.58	5656.8287	5486.3404	-0.0913	-0.2396	0.2564
#5+	11875.73	11458.82	5937.83	5730.17	5937.9597	5730.2178	0.1297	0.0478	0.1382
#6+	11858.36	12307.73	5930.08	6155.25	5930.0410	6155.0472	-0.0390	-0.2028	0.2065
#7+	11035.54	12561.09	5518.17	6281.58	5518.5590	6281.4717	0.3890	-0.1083	0.4038
#8+	11028.00	12064.91	5515.00	6032.92	5514.6869	6033.2863	-0.3131	0.3663	0.4819
#9+	11028.00	12064.91	5515.00	6032.92	5514.6869	6033.2863	-0.3131	0.3663	0.4819
#10+	10639.18	11346.91	5320.00	5673.83	5320.3852	5674.1261	0.3852	0.2961	0.4858

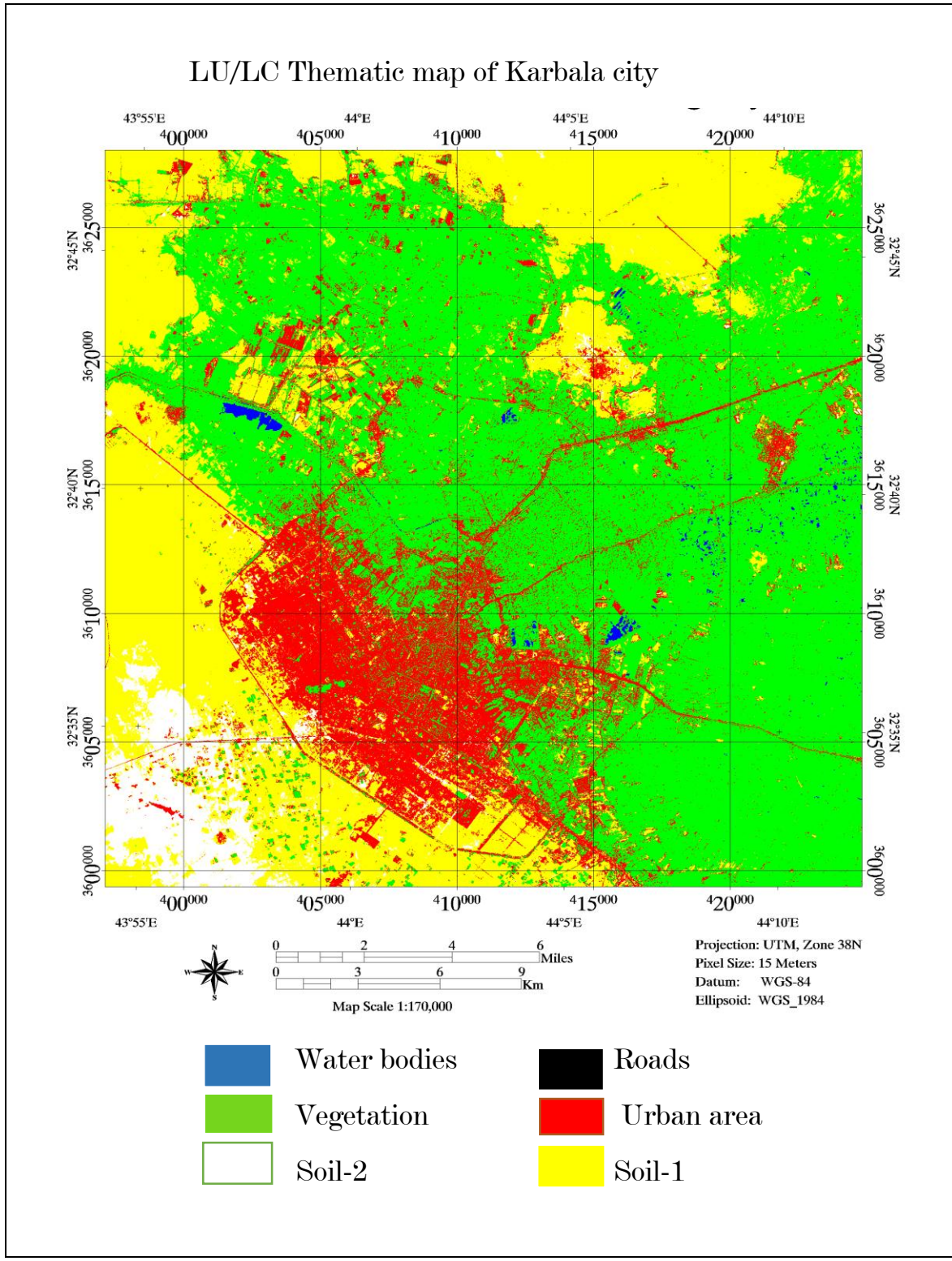

Fig. 13: LU/LC map classified using SVM classified on fused data by Brovey method.

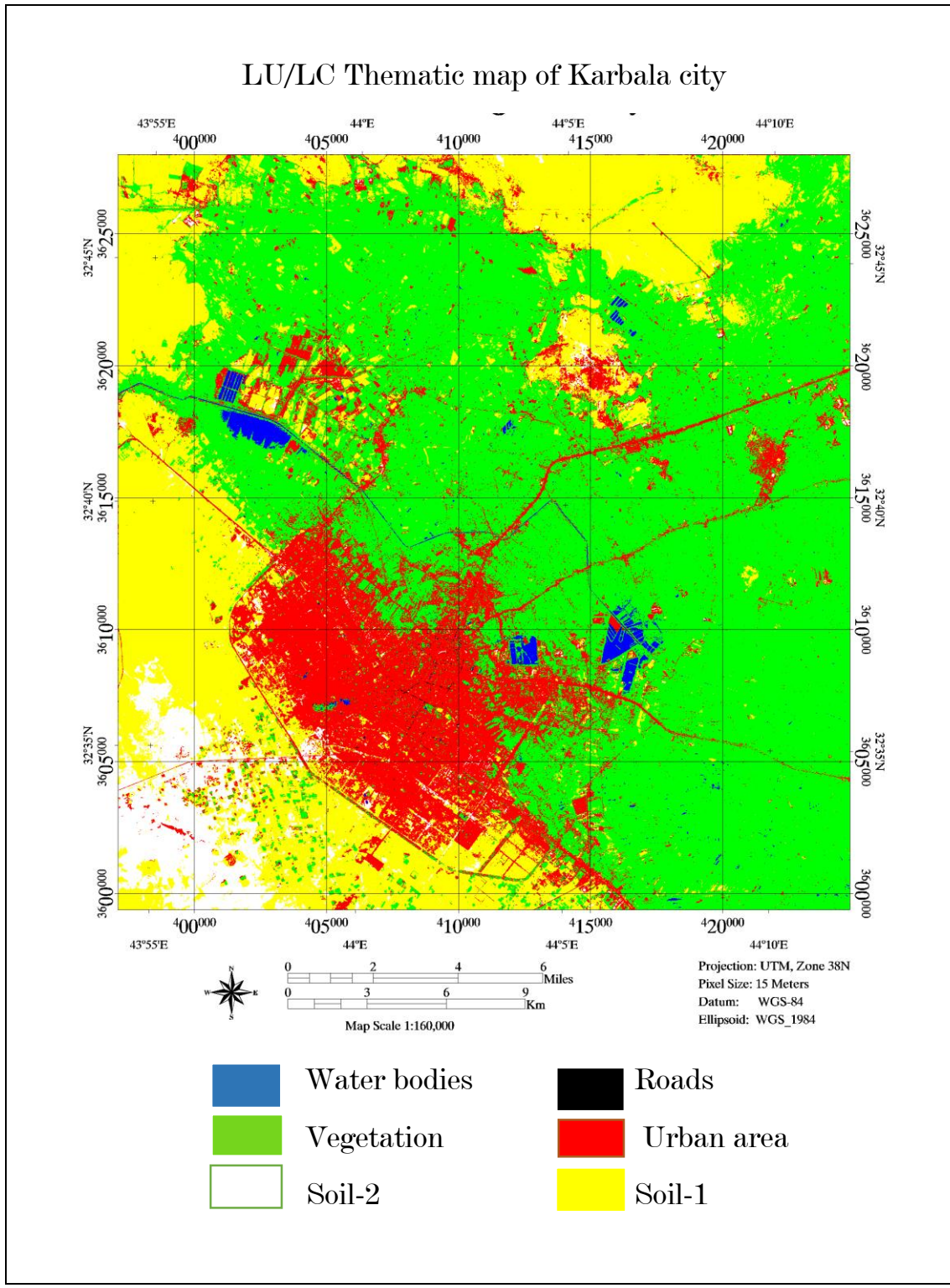

Fig. 14: LU/LC map classified using SVM classifier on fused data by Gram-Schmidt (GS).

Where n is the total number of pixels, n_i represent the number of instances, label (i), that have been classified into the label (j), n_{ij} is a total number of classified pixels. The accuracy of the classification results was evaluated based on the confusion matrix and its coefficients in Tables 6 & 7 which give the classification results fused and classified images by SVM.

Table 6 shows the classification results for the fused image by BT and classifier by the SVM approach, that the Soil-1 classifier got the highest product accuracy of 99.91, and the Soil-2 classifier got the highest accuracy user of 99.96. While the Urban area classifier got the lowest accuracy of product and user 93.64 and 89.32, respectively. As for the rest of the classifiers, they obtained good results, such as the Vegetation classifier, which obtained a product accuracy of 98.39 and user accuracy of 97.87, while the Roads obtained a product accuracy of 96.15 and user accuracy of 95.1, and Waterbodies obtained a product accuracy of 97.99 and user accuracy of 94.14.

Table 7 shows the classification results for the fused image by GS and classifier by the SVM approach, that the Soil-2 classifier got the highest producer accuracy and user accuracy 99.74 and 99.78, respectively. Also, Soil-1 obtained producer and user accuracy of 99.63 and 99.61 respectively, and the Water bodies classifier got the lowest producer accuracy of 86.16. While the Urban area classifier got the lowest user accuracy of 87.37. As for the rest of the classifiers, they obtained good results, such as the Vegetation classifier, which obtained producer accuracy of 98.93 and user accuracy of 97.14, while the Roads obtained producer accuracy of 98.90 and user accuracy of 98.42.

Table 5: Collected training sites from the Landsat-8 satellite image.

Class	Color	Pixels	Polygons
Urban area	Red	4.848	16/4.848
Vegetation	Green	23.275	14/23.275
Water bodies	Blue	6.625	6/6.625
Soil -1	Yellow	19.077	10/19.077
Soil -2	White	8.650	9/8.650
Roads	Black	1.571	By points

Table 6: producer and user accuracies of the fused image by (BT) and classifier by SVM.

Class	Pro. Acc. [%]	User. Acc. [%]
Urban area	93.64	89.32
Vegetation	98.39	97.87
Water bodies	97.99	94.14
Soil-1	99.91	97.52
Soil-2	95.23	99.96
Roads	96.15	95.10

RESULTS AND DISCUSSION

A Fusion process of (MS & Pan) images was carried out in this study to improve the methods of producing LU/LC maps to reach high accuracy. Using sharpening algorithms for the image fusion tool we used Brovey chromatic transformation algorithm and (GS) spatial optimization algorithm and two fusion images were created, and to classify the two images, we relied on the (SVM) method for mapping LU/LC and to make a comparison between the results to estimate which of the two approaches is more accurate, as shown in Figs.13 & 14. We used the confusion matrix to evaluate the results of the (SVM) classification algorithm. Where the value of the kappa coefficient and the overall Accuracy of the (SVM) for fusion images using (GS) are 95 and 97.81%, respectively, and the kappa coefficient and the overall Accuracy of the (SVM) for fusion images using Brovey are 95.15% and 0.93 respectively. By comparing the results and as shown in Table 8, it was shown that the approach used to obtain more accurate and clear LU/LC maps is employing classification for fused images, which is obtained by fusion Landsat-8 satellite (MS & Pan) images by the (GS) sharpening algorithm. Figs. 15 & 16 show the comparison of classification fused images by (BT & GS) at the level of the overall accuracy and Kappa coefficient.

CONCLUSION

The study analyzed the use of Landsat-8 (MS & Pan) images

Table 7: Producer and user accuracies of the fused image by (GS) and classifier by SVM.

Class	Pro. Acc. [%]	User. Acc. [%]
Urban area	97.68	87.37
Vegetation	98.93	97.14
Water bodies	86.16	98.05
Soil-1	99.63	99.61
Soil-2	99.74	99.78
Roads	98.90	98.42

Table 8: Overall accuracy and kappa coefficient of the fused image by (GS and Brovey) and classified by (SVM) classifier.

Type of data	Classifier	Overall accuracy	Kappa coefficient
Fusion image by GS	SVM	97.81%	0.95
Fusion image by BT	SVM	95.15%	0.93

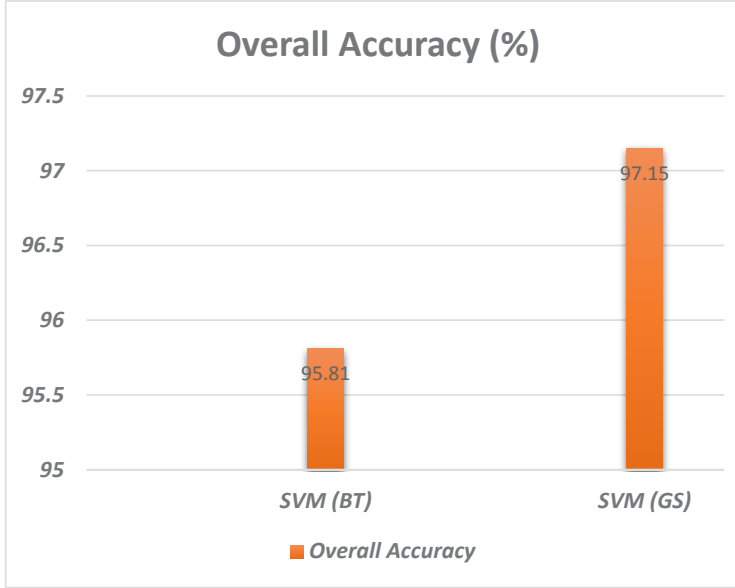

Fig. 15: The overall accuracy of the fused image by (Brovey & GS) and classifier by (SVM).

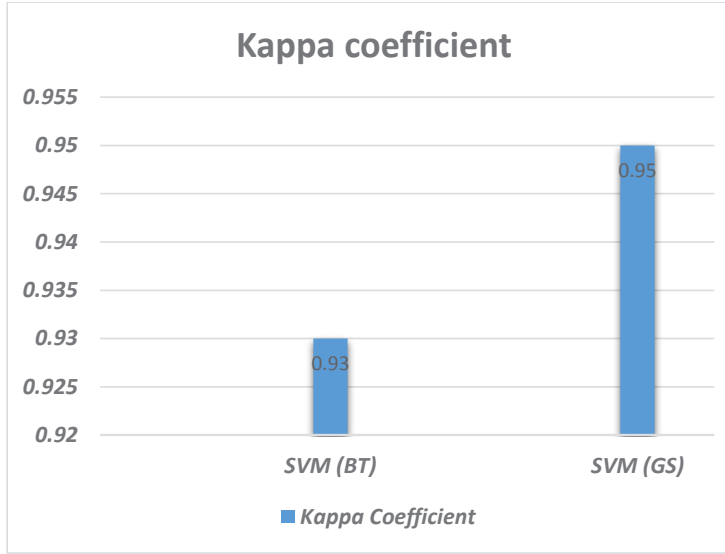

Fig. 16: the Kappa coefficient of the fused image by (Brovey & GS) and classifier by (SVM).

to estimate LU/LC for the city of Karbala, Karbala Governorate, Iraq. This research aims to identify an improved methodology for mapping LU/LC to the city of Karbala by making comparisons between images combined with two methods GS and Brovey classified using SVM. The improved Fused image classifier approach is proposed for LU/LC mapping based on the result by applying a confusion matrix and it shows the full accuracy of the Fused image using spatial optimization algorithm GS and classified by SVM, the highest result with an overall accuracy of 97.81% and kappa coefficient 0.95. Also, results were obtained for the Fused data in the BT method, classified by SVM, overall accuracy of 95.15% and a kappa coefficient of 0.93, Therefore, the image fusion approach using the GS algorithm and classifier by SVM was determined as the best optimized LU/LC mapping technique for this study.

REFERENCES

Abbas, Z. and Jaber, H.S. 2020. Accuracy assessment of supervised classification methods for extraction land use maps using remote sensing and GIS techniques. IOP Conf. Series Mater. Sci. Eng., 16: 54-79

Ali, A.H. and Jaber, H.S. 2020. Monitoring degradation of wetland areas using satellite imagery and geographic information system techniques. Iraq. J. Agric. Sci., 51(5): 1474-1485

Bernstein, L.S., Jin, X., Gregor, B. and Adler-Golden, S.M. 2012. Quick atmospheric correction code: algorithm description and recent upgrades. Optical Eng., 51(11): 111719.

Bouaziz, M., Eisold, S. and Guermazi, E. 2017. Semiautomatic approach for land cover classification: A remote sensing study for the arid climate in southeastern Tunisia. Euro-Mediterr. J. Environ. Integr., 2(1): 1-7.

Cavur, M., Duzgun, H.S., Kemec, S. and Demirkan, D.C. 2019. Land use and land cover classification of Sentinel 2-A: St Petersburg case study. Int. Arch. Photogramm. Remote Sens. Spatial Inform. Sci., 42(1): 16-17

Chasmer, L., Hopkinson, C., Veness, T., Quinton, W. and Baltzer, J. 2014. A decision-tree classification for low-lying complex land cover types within the zone of discontinuous permafrost. Remote Sens. Environ., 143: 73-84. https://doi.org/10.1016/j.rse.2013.12.016.

Dibs, H. 2013. Feature extraction and based pixel classification for estimation of the land cover thematic map using hyperspectral data. Int. J. Eng. Res. Appl., 3(3): 686-693.

Dibs, H. 2018. Comparison of derived Indices and unsupervised classification for AL-Razaza Lake dehydration extent using multi-temporal satellite data and remote sensing analysis. J. Eng. Appl. Sci., 13(24): 1-8.

Dibs, H. and Al-Hedny, S. 2019. Detection of wetland dehydration extent with multi-temporal remotely sensed data using remote sensing analysis and GIS techniques. Int. J. Civil Eng. Technol., 10: 143-154.

Dibs, H., Al-Hedny, S. and Karkoosh, H.A. 2018. Extracting detailed buildings 3D model using high-resolution satellite imagery by remote sensing and gis analysis: Al-Qasim Green University a case study. Int. J. Civil Eng. Technol., 9(7): 1097-1108.

Dibs, H., Hasab, H.A., Al-Rifaie, J.K. and Al-Ansari, N. 2020. An optimal approach for land-use/land-cover mapping by integration and fusion of multispectral Landsat OLI images: A case study in Baghdad, Iraq. Water Air Soil Pollut., 231(9): 1-15.

Dibs, H., Hasab, H.A., Jaber, H.S. and Al-Ansari, N. 2022. Automatic feature extraction and matching modelling for highly noise near-equatorial satellite images. Innovative Infrastructure Solutions, 7(1), pp.1-14.

Dibs, H., Hasab, H.A., Mahmoud, A.S. and Al-Ansari, N. 2021. Fusion methods and multi-classifiers for improving land cover estimation by remote sensing analysis. Geotech. Geolog. Eng., 39: 5825-5842.

Dibs, H., Hasab, H.A., Mahmoud, A.S. and Al-Ansari, N. 2021. Fusion Methods and Multi-classifiers to Improve Land Cover Estimation Using Remote Sensing Analysis. Geotechnical and Geological Engineering, 39(8), pp.5825-5842.

Erener, A., 2013. Classification method, spectral diversity, band combination and accuracy assessment evaluation for urban feature detection. International Journal of Applied Earth Observation and Geoinformation, 21, pp.397-408.

Gevana, D., Camacho, L., Carandang, A., Camacho, S. and Im, S. 2015. Land use characterization and change detection of a small mangrove area in Banacon Island, Bohol, the Philippines using a maximum likelihood classification method. Forest Sci. Technol., 11(4): 97-205.

Hasab, H.A., Dibs, H., Dawood, A.S., Hadi, W.H., Hussain, H.M. and Al-Ansari, N. 2020a. Monitoring and assessment of salinity and chemicals in agricultural lands by a remote sensing technique and soil moisture with chemical index models. Geosci., 10(6): 207.

Hasab, H.A., Jawad, H.A., Dibs, H., Hussain, H.M. and Al-Ansari, N. 2020b. Evaluation of water quality parameters in marshes zone southern of Iraq based on remote sensing and GIS techniques. Water Air Soil Pollut., 231(4): 1-11.

Idi, B.Y. and Nejad, P.G. 2013. Fusion of RADARSAT-2 and IKONOS images for land cover mapping: Performance analysis. Appl. Remote Sens. J. 3(1): 18.

Iounousse, J., Er-Raki, S., El Motassadeq, A. and Chehouani, H. 2015. Using an unsupervised approach of probabilistic neural network (PNN) for land use classification from multitemporal satellite images. Appl. Soft Comput., 30: 1-13. https://doi.org/10.1016/j.asoc.2015.01.037.

Jasem, I.T. and AL-Mayali, S.F. 2020. The geographical potential of agricultural tourism in Karbala governorate. J. Univ. Babylon Human., 28(11): 189-209.

Jawak, S.D. and Luis, A.J. 2013. A comprehensive evaluation of PAN-sharpening algorithms coupled with resampling methods for image synthesis of very high resolution remotely sensed satellite data. Adv. Remote Sens., 61: 2013.

Jia, M., Wang, Z., Li, L., Song, K., Ren, C., Liu, B. and Mao, D. 2014. Mapping China's mangroves based on an object-oriented classification of Landsat imagery. Wetlands, 34(2): 277-283. https://doi.org/10.1007/s13157-013-0449-2.

Kumar, L., Sinha, P. and Taylor, S. 2014. Improving image classification in a complex wetland ecosystem through image fusion techniques. J. Appl. Remote Sens., 8(1): 083616.

Li, G., Lu, D., Moran, E., Dutra, L. and Batistella, M. 2012. A comparative analysis of ALOS PALSAR L-Band and RADARSAT-2 C-band data for land-cover classification in a tropical moist region. J. Photogramm. Remote Sens., 70: 26-38. https://doi.org/10.1016/j.isprsjprs.2012.03.010.

Löw, F., Conrad, C. and Michel, U. 2015. Decision fusion and non-parametric classifiers for land use mapping using multitemporal Rapideye data. J. Photogramm. Remote Sens., 108: 191-204. https://doi.org/10.1016/j.is

Mandhare, R.A., Upadhyay, P. and Gupta, S. 2013. Pixel-level image fusion using brovey transform and wavelet transform. Int. J. Adv. Res. Electr. Electr. Instrument. Eng., 2(6): 2690-2695.

Otukei, J.R., Blaschke, T. and Collins, M. 2015. Fusion of Terrasar-X and Landsat ETM+ data for protected area mapping in Uganda. Int. J. Appl. Earth Observ. Geoinform., 38: 99-104. https://doi.org/10.1016/j.jag.2014.12.01

Sameen, M.I., Nahhas, F.H., Buraihi, F.H., Pradhan, B. and Shariff, A.R.B.M. 2016. A refined classification approach by integrating Landsat Operational Land Imager (OLI) and RADARSAT-2 imagery for land-use and land-cover mapping in a tropical area. Int. J. Remote Sens., 37(10): 235

Sang, H., Zhang, J., Zhai, L., Qiu, C. and Sun, X. 2014. Analysis of rapid eye imagery for agricultural land cover and land use mapping. In: 2014 3rd International Workshop on Earth Observation and Remote Sensing Applications (EORSA), IEEE, Changsha, pp.366-369.

Sarp, G. 2014. Spectral and spatial quality analysis of pan-sharpening algorithms: A case study in Istanbul. Europ. J. Remote Sens., 47(1): 19-28.

Tabib Mahmoudi, F. and Karami, A. 2020. Quantitative assessment of transformation-based satellite image pan-sharpening algorithms. J. Electr. Comput. Eng. Innov., 8(2): 161-168.

Zhang, N., Zhao, J. and Zhang, L. 2016. Comparison and evaluation of image fusion methods for GaoFen-1 imagery. Infrared Technol. Appl. Robot Sens. Adv. Contr., 101: 101571.